A comparison of structure-activity of Cu-modified over different mesoporous silica supports for catalytic conversion of levulinic acid

Balla Putrakumar[a,*], Seelam Prem Kumar[b*], Ginjupalli Srinivasarao[c], Karthikeyan Rajan[a], Mitta Harishekar[d], Keiski Riitta[b], Tong Xiang Liang[a,*]

a- Engineering Research Centre for Hydrogen Energy and New Materials, College of Rare Earths (CORE), Jiangxi University of Science and Technology, Ganzhou 341000, China.

b- Environmental and Chemical Engineering, Faculty of Technology, P.O. Box 4300, University of Oulu, Finland.

c- Applied Chemistry section, Department of Applied Sciences, University of Technology and Applied Sciences, Muscat, P.O. Box 74, P.C 133, Oman.

d- Catalysis Division, Indian Institute of Chemical Technology, Hyderabad, India

---

* Corresponding authors: Dr. Putrakumar Balla and Prof. Tong Xiang Liang, Engineering Research Centre for Hydrogen Energy and New Materials, College of Rare Earths (CORE), Jiangxi University of Science and Technology, Ganzhou, China, 341000.
E-mail: bputrakumar@yahoo.com; txliang@jxust.edu.cn

Dr. Prem Kumar Seelam, Environmental and Chemical Engineering, Faculty of Technology, P.O.Box 4300, University of Oulu, Finland. E-mail prem.seelam@oulu.fi

Abstract

Catalytic hydrogenation of levulinic acid (LA) to γ-valerolactone (GVL) was investigated over four different types of mesoporous silica (SBA-15, MCM-48, MCM-41, and KIT-6) supported copper (5 wt.%) catalysts. The Cu was incorporated into mesoporous silica supports by a sequential impregnation method. A detailed investigation of the support structure-activity correlation and the performance of the catalysts in LA conversion was studied. Detailed characterisation techniques were used to evaluate the physical and catalytic properties of the studied catalysts. The structure type and physicochemical properties of the silica support had a significant effect on the overall performance of the catalysts. Among them, over Cu/SBA-15 catalyst, a complete levulinic acid (LA) conversion with ~98%

gamma valerolactone (GVL) selectivity was achieved at 265°C under ambient H_2 pressure. The superior performance of Cu/SBA-15 catalyst was attributed to the high surface acidity, reducibility of Cu oxides species, and highly dispersed Cu particles over SBA-15 structure. The results confirmed that the activity of the catalysts is significantly influenced by the textural properties, surface acidity and copper dispersion. Durability of all the catalysts were also tested for 50 h time on stream and over SBA-15 catalyst, only a small drop in the activity was observed.

Keywords: Copper, Mesoporous silica, Levulinic acid, γ-Valerolactone,

Introduction

Levulinic acid (LA) has been considered as one of the most versatile and renewable molecules produced from hydrolysis of lignocellulosic biomass conversion. It has a great potential platform chemical in biorefinery applications **[1-4].** Due to this, considerable efforts are being made and multiple strategies are being proposed for the efficient conversion of LA to value-added compounds and fuels. Among the various transformations of LA, catalytic hydrogenation of LA to γ-valerolactone (GVL) is an important route in the valorisation of biomass platform molecules to specialty chemicals **[5-7].** Gamma valerolactone has been used widely as a sustainable liquid feedstock in the production of transportation biofuels and also as a fuel additive to gasoline/ethanol mixture. Further, GVL act as a potential monomer in the manufacturing of different kinds of plastics and it can be directly utilized as a green solvent **[8,9]**. Moreover, GVL has been used as a hydrogen carrier in the fuel cell applications and also used as a 20% biofuel (produced from GVL) balanced with conventional gasoline in the biofuel engine and also used in the production of non-enzymatic sugars from biomass conversion.

Catalytic hydrogenation of LA to GVL were studied over a wide variety of noble (Ru, Pt, Pd, Au, and Ir) **[10-14]**, non-noble (Cu, Ni, and Co) **[15-17]** and bimetallic (RuNi, RuSn,CuFe and CuNi) **[18-21]** catalysts in both continuous and batch reactor systems under various reaction conditions. Among the catalysts reported, ruthenium (Ru) based catalytic systems are considered to be the most active and selective in the conversion of LA to GVL in both *i.e.*, homogenous and heterogeneous media **[20]**. Many reports are focused on non-noble based metal catalysts due to their cost and abdundance. Developing Cu-based catalysts is more appropriate and industrially viable for the future biorefinery applications. The copper based catalysts are considered to be promising alternatives to the noble metal catalysts, which have shown moderately high performance in the catalytic transformation of LA to GVL. For instance, Upare *et al.* reported a 5 wt.% Cu/SiO_2 catalyst exhibited a complete conversion of LA with ~94% GVL selectivity and 6% angelica lactone (AL) at 265°C and 0.1 MPa **[22]**. Lomate *et al.* 2017 studied the effect of Cu modified SiO_2 support with different textural properties of SiO_2 and exhibited different activities in vapor phase hydrogenation of levulinic acid. However, they found that no correlation between activity and selectivity with support acidity, but strong Cu-support interactions due to partially oxidised Cu species was the main reason for the high activity **[23]**. Moreover, Rei *et al.*, used a 20 wt.% Cu/SiO_2 catalyst, and achieved ~73.4% LA conversion with ~75.4% GVL selectivity at 250°C and WHSV of 3.30 h^{-1}**[24]**. Recently, Sun *et al.* studied three different non-noble metal catalysts *i.e.*, Co, Ni, and Cu based alumina catalysts. Overall, Cu/Al_2O_3 was found to be the most selective catalyst due to the high surface acidity and Cu dispersion **[25].** Furthermore, in another study, Cu/Al_2O_3 and Cu/ZrO_2 catalysts were reported in the hydrogenation of LA in a fixed bed reactor at 265°C under ambient pressure and highest catalytic activity in terms of GVL selectivity and LA conversion was gained over Cu/Al_2O_3 catalyst **[26, 27]**. Most of the studies, the GVL selectivity was directly correlated to the active metal surface area, surface

acidity, and the metal dispersion. Henceforth, designing and developing a highly dispersed, low cost and abundant Cu-based catalyst in combination with a robust support was the aim of this work..

Generally, mesoporous silica supports (SBA-15, MCM-41, MCM-48, and KIT-6) possess high specific surface areas, ordered pore structures, and high thermal stability, which makes them ideal materials for many catalytic reactions. High surface area mesoporous silica (MS) supports can efficiently provide the maximum active sites per mass of catalyst. Moreover, MS supports avoid the diffusion limitations for the reactants and products due to their unique textural properties. However, changing the textural and surface properties of different mesoporous materials can lead to varied catalytic performances **[28]**.

The aim of the work is to study the Cu loaded different mesoporous silica supported catalysts with different textural properties in a fixed bed reactor at ambient pressure was performed. Thus, this work gives an overall correlation between the role of MS textural properties, metal-support interaction, copper dispersion with the catalytic activity. In the present work, four different types of mesoporous silica supports were synthesized by a hydrothermal method and then copper nanoparticles were deposited by a sequential wet impregnation method. The catalysts characterized by using various techniques and methods such as microscopic, spectroscopic, XRD, UV-DRS, N_2 sorption measurements, SEM, TEM, H_2-TPR, and NH_3-TPD. Active surface area and dispersion of copper were calculated from the N_2O titration method. Catalytic activities were determined in terms of LA conversion, GVL selectivity and catalysts stability.

Experimental

Materials and methods

The following chemicals and reagents were used in this work: P123 (Poly(ethylene glycol)-*block*-poly(propylene glycol)-*block*-poly(ethylene glycol) (Sigma Aldrich), Potassium Chloride, Tetra Ethyl Orthosilicate (TCI chemicals, >97%), Hydrochloride, Cetyl Trimethyl Ammonium Bromide (Sigma Aldrich, 98%) , Ethanol (Analytical grade), Ammonia solution (30%), Copper nitrate (Sigma Aldrich, 98%) and Deionized water.

The parent silica materials (SBA-15, MCM-41, MCM-48, and KIT-6) were synthesized from the study **[29]**. In the synthesis of SBA-15, 4 g of P123 (Poly(ethylene glycol)-*block*-poly(propylene glycol)-*block*-poly(ethylene glycol) polymer and 9.44 g of KCl were dissolved in 2 M HCl solution (~90 g). The final solution was stirred for 2 h at 35°C until homogeneously mixed. In the next step, 6.44 g of TEOS (Tetraethyl orthosilicate) was added dropwise under continuously stirring for 2 h. The complete mixture was then transferred to a sealed Teflon lined container and kept at 100°C for 24 h under static conditions. The resulting precipitate was filtered and washed with deionised water (pH 6.9±0.2) until pH 7.0±0.2 was attained. Further, it was dried for 12 h at 80°C and followed by calcination at 500°C for 6 h under air.

For MCM-48, 2.4 g of CTAB (Cetyltrimethylammonium bromide) was mixed with 50 mL of deionized water, 50 mL of C_2H_5OH and 12 mL of NH_3 (32 vol.%). This mixture was stirred until a clear solution was obtained. In the next step, TEOS (3.4 g) was added to the mixture and stirred for 2 h. The final product was filtered, thoroughly washed, and dried overnight, and finally, calcined for 6 h at 600°C.

The MCM-41 support was prepared by using 2.4 g of CTAB dissolved in 120 mL of deionized water and then stirred until a clear solution was visible. After dissolution, 8 mL of NH_3 (32%) was added to the solution, followed by dropwise addition of 10 mL of TEOS and

stirring at 35°C for 24 h. The final product was washed with ethanol/H_2O, dried for 12 h at 60°C and calcined for 5 h at 500°C.

For the synthesis of KIT-6, Pluronic P123 (6 g) was dissolved in 215 mL of deionized water and 11.8 g of HCl (~35% v/v) solution under stirring. After dissolution, a 6 g of n-butanol was added dropwise under continuous stirring. In the next step, a TEOS (12.9 g) was added and stirred at 35°C for 24 h. The final solution was transferred into a sealed Teflon container and subjected to hydrothermal treatment at 100°C for the whole one day. The final solid product was washed, filtered, and dried overnight and then calcined at 500°C for 5 h.

The supported copper catalysts with 5 wt.% Cu loading was prepared by a sequential wetness impregnation method. In the typical synthesis procedure, 1.0 g of mesoporous silica support (SBA-15, MCM-41, MCM-48, and KIT-6) was dispersed in 20 mL of aqueous copper nitrate solution and stirred at 60°C. The samples were dried overnight and calcined at 500°C for 5 h. The prepared catalysts were labeled as Cu/SBA-15, Cu/MCM-41, Cu/MCM-48 and Cu/KIT-6.

Catalyst Characterisation

X-ray diffraction patterns were obtained by a D8 X-ray diffractometer (Bruker, Germany) using Cu Kα radiation (-1.5406 A°, 40 kV and 30 mA). Nitrogen sorption measurements were conducted on a Autosorb-1 analyzer (Quanta chrome) at -196^{o}C. Before analysis, the samples were degassed at 250°C for 6 h under vacuum. The specific surface area and pore size distribution were measured by using Brunauer-Emmett-Teller (BET) and Barret-Joyner-Halenda (BJH) methods, respectively. The UV-Vis diffused reflectance spectra (UV-DRS) were recorded by a UV-visible spectrometer (GBC, scientific-Cintra). Transmission electron microscopy (TEM) images were captured on a Hitachi HT7700 operated at 100 kV instrument. Scanning electron microscopy (SEM) images were taken on a Philips/Fei Quanta 200F SEM operated at 20 kV instrument.

Hydrogen temperature programmed reduction (H_2-TPR) and temperature programmed desorption of NH_3 (NH_3-TPD) were conducted on a micrometric instrument (Auto Chem. 2910). In H_2-TPR experiment, typically 0.1 g of sample was pretreated by passing He gas at 200°C for 2 h and then cooled down to ambient temperature. TPR analysis was performed from 25°C to 600°C under the flow of 5 vol.% H_2/Ar with a ramping rate of 10°C/min. Moreover, in NH_3-TPD experiment, 0.1 g sample was pretreated by a flow of He gas at 200°C for 2 h followed by saturation with 10% NH_3/He gas at 80°C for 1 h. The samples were then purged with He gas at 140°C for 2 h. TPD analysis was carried out from 25°C to 600°C at a ramping rate of 10°C/min and Grams/32 software was used to calculate the amount of H_2 consumed for TPR and desorbed NH_3 values for TPD analysis.

N_2O decomposition experiments were also conducted on a micrometric instrument (Auto Chem.2910). Prior to the analysis, the sample was reduced under H_2 flow at 300°C for 3 h followed by He purge for 30 min and then cool down to 80°C. Thereafter, the sample was exposed to 2 vol.%N_2O-He for 30 min to oxidize the Cu to Cu_2O. Reduction of surface copper oxides was performed by a similar procedure for the TPR experiments. The Cu surface area, dispersion and crystal size were measured from the total amount of N_2O consumed during the decomposition experiments. Copper metal surface area of the catalyst were determined by the following equation.

$$\mathbf{S_{cu} = N_M \times N_A \times SF / Ns}$$

where S_{cu} is the Metal surface area ($m^2.g^{-1}$), $\mathbf{N_M}$ is the Gas adsorbed at monolayer, $\mathbf{N_A}$ is the Avogadro number, **SF** is the Adsorption stoichiometry, and **Ns** is the Number of surface copper atoms per unit area (1.47×10^{19} m^{-2}).

By assuming copper metal to be spherical crystallites, the particle size can be calculated from following equation: Particle size (Å) = $6\times10^4 / (\mathbf{S}_{Cu}.\boldsymbol{\rho}_{Cu})$

where ρ_{Cu} is the copper density (8.92 $g.cm^{-3}$).

Catalytic activity

The catalytic hydrogenation of LA was performed in a fixed-bed glass reactor with 9 mm inner diameter and 32 cm in length over a temperature range from 225 to 300°C at 0.1 MPa hydrogen pressure. The catalyst (0.3 g) was mixed with glass beads and loaded at the center of the reactor with glass wool packed from both ends. Before the activity test, the catalyst was pretreated with H_2 stream at 350°C for 3 h. After the reduction, the reactor temperature was cool down to 265°C and a stream of aqueous solution (10 wt.%) of LA was fed into the reactor along with H_2 at WHSV 0.550 h^{-1}. The reaction products were collected after every hour in an ice trap and later analyzed by GC-MS (HP5973-GC-MSD) by using capillary column (HP-1MS).

Results &discussion

Characterisation results

Low angle XRD patterns of four pure supports (SBA-15, MCM-41, MCM-48, and KIT-6) and their respective Cu impregnated samples have been presented in Figure. 1a and inset in Fig. 1a, respectively. The low-angle diffraction patterns of SBA-15 and Cu/SBA-15 exhibited well-resolved diffraction peaks at around 2θ-0.9° corresponds to (1 0 0) reflection of SBA-15 **[30]** and indicating a hexagonal unit cell. The results confirmed that the mesoporous silica structure was well intact after the copper incorporation. However, the impregnation of copper on the silica support resulted in a low intensity peak, which could be ascribed to the scattering phenomenon of metallic copper nanoparticles.

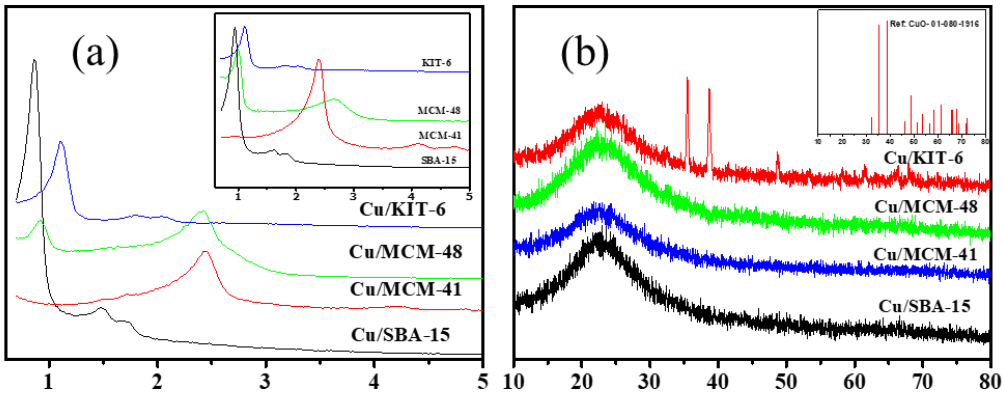

Figure 1. Low angle XRD patterns of various (a) mesoporous silica supported copper catalysts and (inset Figure 1a) parent mesoporous silica and (b)wide angle XRD pattersof various mesoporous silica supported copper catalysts.

The XRD pattern of pure MCM-41 (inset in Fig.1a) shows all three well-separated reflections at 2θ-3.7° (a strong intense peak), around 2θ-4.5°, and 2θ-4.7° denoted as weak intense peaks, corresponding to d_{100}, d_{110} and d_{200} planes, respectively, which was considered as the fingerprints of ordered mesoporous Si structures [31] of MCM-41 material. After the impregnation of copper over the MCM-41 support, the intensity of all XRD peaks decreased considerably due to occupied Cu species in the cylindrical mesopores of the MCM-41 support. The diffraction peaks of MCM-48 and Cu/MCM-48 were shown in good agreement with the unique 3D cubic structures of MCM-48, as reported elsewhere [32]. Moreover, KIT-6 catalyst exhibited well-resolved reflections, which were assigned to a well-ordered 3-D cubic Ia3d symmetry of silica structure [33]. Further, the 5 wt.% Cu/KIT-6 catalyst manifested a cubic structure, which was very similar to its parent sample. All Cu impregnated mesoporous Si catalysts exhibited a declining steadily in their diffraction peaks intensities as compared to their respective parent bare samples.

Table 1. Textural properties of different mesoporous silica support and the Cu modified catalysts.

Catalyst	Copper loading[a] (wt. %)	BET surface area[b] (m^2/g)	Pore volume[b] (cc/g)	Average pore diameter[b] (nm)
SBA-15	-	1062	1.413	5.10
MCM-41	-	759	0.692	3.65
MCM-48	-	1125	0.6075	2.16
KIT-6	-	767	0.8969	4.67
Cu/SBA-15	4.61	764	0.9137	4.78
Cu/MCM-41	4.48	693	0.5971	2.67
Cu/MCM-48	4.51	928	0.5669	2.06
Cu/KIT-6	4.57	524	0.7567	5.77

a-Results obtained from ICP
b-Results obtained from N_2 sorption measurements

The wide-angle XRD patterns of the supported copper catalysts have been illustrated in Fig. 1b. All the XRD patterns shown broad peaks between 2θ =15-30°, which were considered as characteristic peaks of amorphous silica structure. Further, Cu/KIT-6 shown distinguished peaks correspond to CuO (JCPDS 45-0937) at 2θ = 32.63°, 35.54°, 38.85°, 48.95°, 53.61°, 58.54°, and 61.73°, respectively. The observed peaks indicated that the presence of bulk CuO in KIT-6, however, similar peaks were absent in Cu/SBA-15, Cu/MCM-41and Cu/MCM-48 catalysts. The results suggested that CuO crystallites were highly dispersed over Cu/SBA-15, Cu/MCM-41 and Cu/MCM-48 catalysts and formed smaller Cu crystallites (< 4nm) over the respective supports.

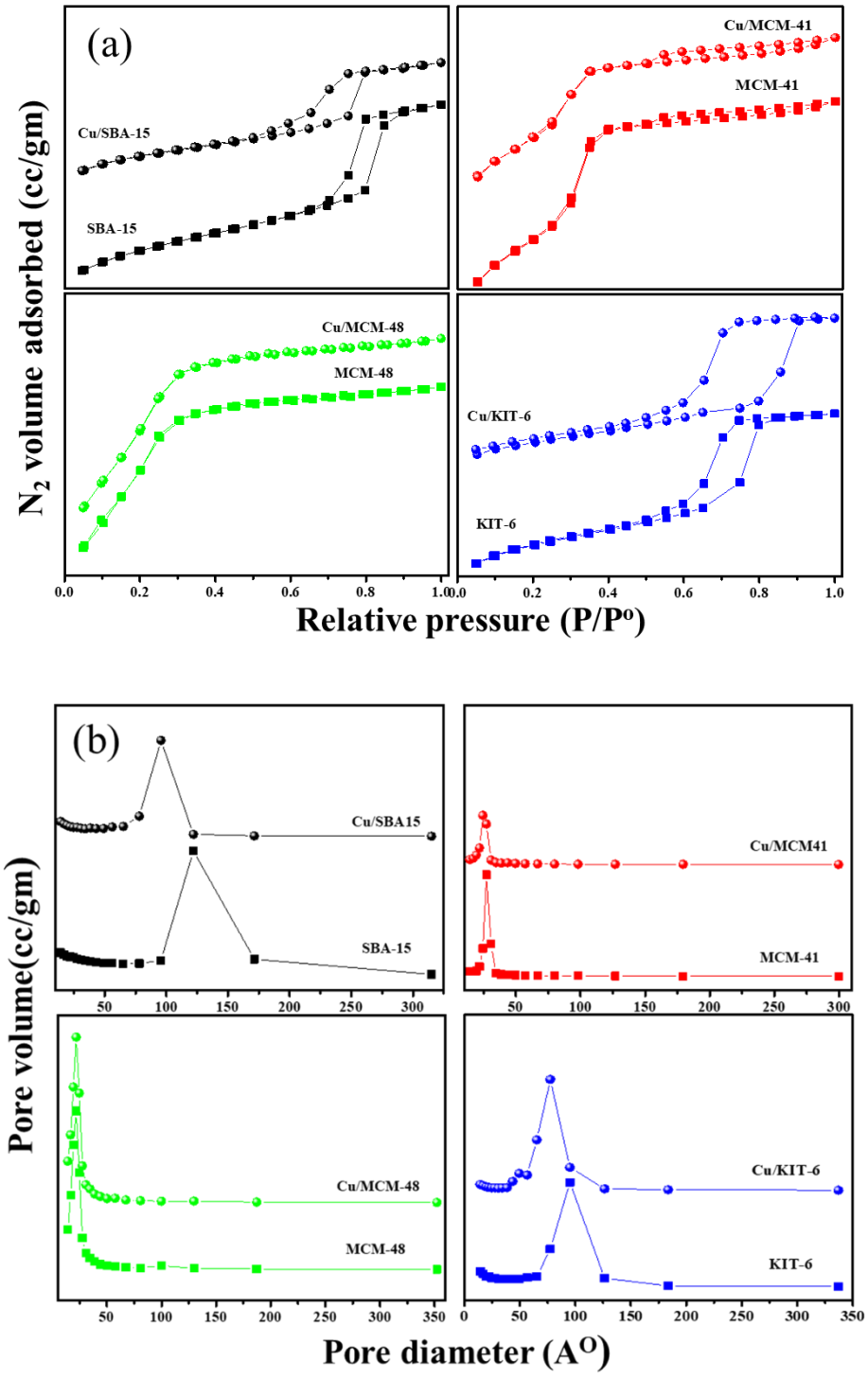

Figure 2. (a) Nitrogen sorption isotherms and the (b) BJH pore size distribution of mesoporous silica supports and the copper supported silica based catalysts.

Moreover, N_2 adsorption-desorption analysis was carried out to determine the specific surface area, cumulative pore volume and average pore size of the prepared catalysts. N_2

sorption isotherms and the respective BJH pore size distribution profiles of pure supports and supported copper catalysts have been presented in Fig. 2a and Fig. 2b. For all four supported catalysts, a sharp enhancement in the N_2 adsorption and desorption isotherms were displayed in the relative pressure range of 0.6-0.7 for SBA-15, 0.3-0.35 for MCM-41, 0.25-0.35 for MCM-48 and 0.5-0.8 for KIT-6, respectively **[34, 35]**. The isotherms of pure SBA-15 and Cu/SBA-15 exhibited a sharp uptake of N_2 at relative pressures of 0.6-0.8, presenting a type IV isotherm with H1 hysteresis loop. This indicated the presence of evenly distributed cylindrical narrow pores in the SBA-15. The isotherms of pure MCM-41 support and Cu/MCM-41 exhibited a typical type IV isotherm with definite elevation in P/P_o range of 0.25-0.35 and 0.3-0.4 due to capillary condensation and spontaneous filling of mesopores, respectively. The isotherm of MCM-48 presented a sharp adsorption at relative pressure of ~0.25, representing a narrow distribution of pores. The specific surface area, pore volume and average pore diameter declined significantly after copper incorporation *i.e.*, supported catalysts Cu/SBA-15, Cu/MCM-41 and Cu/MCM-48 compared to pure support materials (Table 1). The incorporation of copper into mesopores resulted in increased density of Cu/CuO sites and thus, a considerable decreasing amount of surface area of silica support material was observed. However, in the case of Cu/KIT-6, the average pore diameter was slightly increased, which ascribed by the blocking of the smaller pores **[29]**.

The UV-DRS spectra of all the supported catalysts have presented in Figure 3. All the catalysts exhibited one common intense absorption band ranging from 200 to 280 nm, which could be originated from the charge transfer transition between ligand O^{2-} and Cu^{2+} in an isolated state **[36]**. Further, a slight shoulder peak was also observed for the Cu/SBA-15, Cu/MCM-48 and Cu/KIT-6 catalysts at around 300 nm, indicating the limited presence of oligomeric cluster-like moieties originating from the charge transfer between Cu^{2+} and O^{2-} in the $(Cu\text{-}O\text{-}Cu)_n$ surface species **[37]**. The charge transfer band of Cu/MCM-48 was found to

be more intense and broader compared to other catalysts indicating the formation of mononuclear oxide species in a dispersed state. The broad absorption band with weak intense band was observed between 500-800 nm, and this band was assigned to electron d–d transitions in Cu_{2p} in a octahedral surrounding by the oxygen atoms in the CuO particles **[38].**

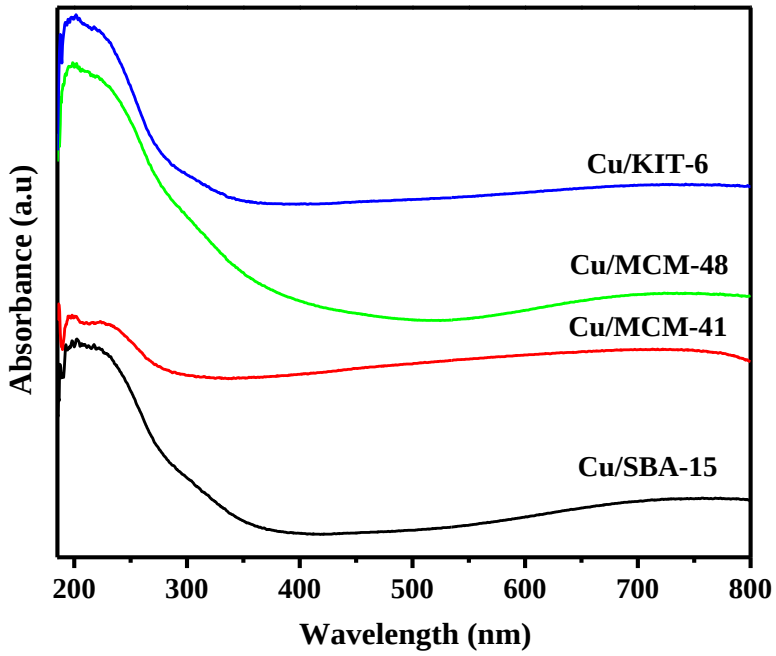

Figure 3. UV-DRS spectra of CuO supported mesoporous silica catalysts.

The TPR profiles and their respective hydrogen consumption values of the supported copper catalysts have been presented in Fig. 4 and Table 2 respectively. From Fig. 4, herein, two similar reduction peaks at ~220°C and ~290°C were observed for Cu/SBA-15 and Cu/MCM-48 catalysts, respectively. The low temperature peak was corresponding to a finely dispersed reduced CuO to Cu sites, while the high temperature peak was originated from the reduction of bulk CuO species presented in the mesoporous silica support structure.

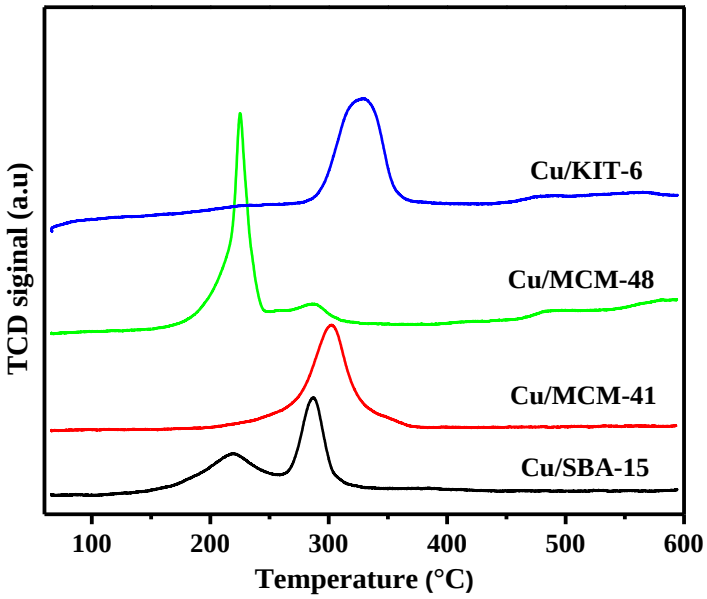

Figure 4. TPR profiles of CuO supported mesoporous silica catalysts.

The published reports related to the reducibility of supported copper catalysts have suggested that bulk CuO is hard to reduce as compared to the highly dispersed copper oxides **[39].** In many studies, similar peaks at ~220°C and ~290°C in Cu/MCM-48 were detected and these peaks corresponds to widely dispersed CuO species over support surface and the bulk CuO species presented inside the structure, respectively. The TPR profiles for the Cu/MCM-41 and Cu/KIT-6 catalysts consist a single reduction peak in high temperature region (i.e., around 310°C). The profile for Cu/MCM-41 corresponds to the reduction of bulk CuO to metallic copper, while the reduction profile of Cu/KIT-6 suggested the shifting of peak towards higher temperature region due to the existence of copper oxides in the bulk of the support structure. Typically, H_2 consumption values for C/SBA-15 and Cu/MCM-48 in a low temperature region was found to be relatively high compared to all other catalysts. Thus, indicates that the most of CuO species were highly dispersed over the MCM-48 and SBA-15 supports and that could be easily reducible. The results were found to be in well agreement with the XRD, UV-DRS, and textural properties.

Table 2. The maximum peak temperature (T_{max}) and hydrogen consumption values of various copper-based catalysts from H_2-TPR analysis and NH_3 desorption values from NH_3-TPD results.

Catalyst	T max[1] (^{0}C)	H_2 consumption (μmol/gm)	T max[2] (^{0}C)	H_2 consumption[a] (μmol/gm)	Total H_2 Consumption[a] (μmol/g)	Total desorbed[b] NH_3 (μmol/g)
5Cu/SBA-15	220	96	290	456	552	837
5Cu/MCM-41	-	-	301	482	482	564
5Cu/MCM-48	200	487	279	36	523	671
5Cu/KIT-6	-	-	318	543	543	441

a-Results from H_2-TPR
b-Results obtained from NH_3-TPD

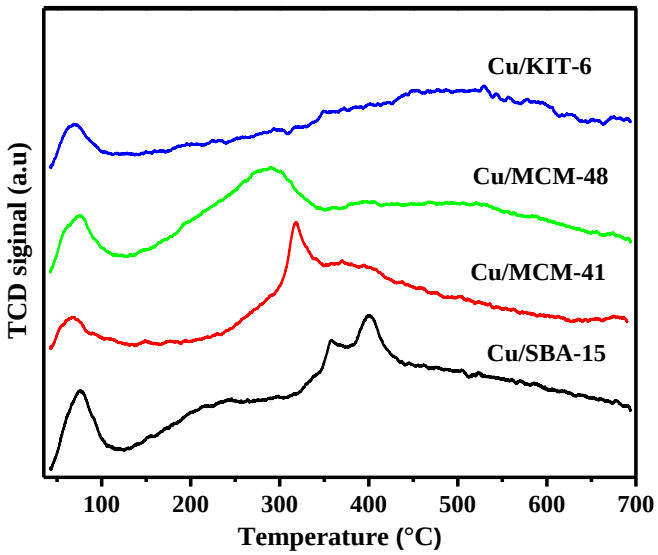

Figure 5. NH_3-TPD profiles for CuO supported mesoporous silica catalysts.

The TPD profiles for copper supported catalysts have shown in Fig. 5 and corresponding data have been summarized in Table 2. All the four catalysts showed one desorption peak below 120°C, that is due to the physisorbed NH_3 over the surface of the catalyst. The Cu/SBA-15 and Cu/MCM-48 exhibited a shoulder peak in between 120-300°C, which was attributed to the desorption of ammonia from the weak acid sites **[40].** All the

catalysts exhibited broad desorption peaks at higher temperature (*i.e.*, above 300°C) due to the existence of moderate acid sites on the surface. The weak to moderate strength acid sites are predominantly higher in Cu/SBA-15 catalyst. Further, the total surface acidity of the supported mesoporous silica catalysts was found to be in the sequence of Cu/SBA-15>Cu/MCM-48> Cu/MCM-41> Cu/KIT-6 (Table 2).

Copper dispersion has been defined as the ratio of the number of copper atoms present over the surface to the total number of copper atoms. The copper dispersion, active metal surface area and crystallite size of copper supported silica catalysts were reported in Table 3. According to the N_2O decomposition results, the H_2 uptake, Cu dispersion, and Cu metal area over the mesoporous silica-supported copper catalysts were presented in the decreasing order: Cu/MCM-48>Cu/SBA-15>Cu/MCM-41>Cu/KIT-6. It was observed that over Cu/MCM-48 catalyst, exhibited highest copper surface area and better dispersion compared to all other catalysts (Table 3). The reason for this might be due to the presence of high number dispersed copper sites over Cu/MCM-48 surface. The Cu/SBA-15 and Cu/MCM-48 exhibited almost similar and moderately high dispersion and active area and moreover, Cu/KIT-6 presented low dispersion due to lower surface area and bigger pore diameter, thus, Cu sites mostly presented inside the pore network (sites which are inaccessible during reactions).

Table 3. Copper dispersion, metal surface area and particle size of different copper supported mesoporous silica catalysts.

Catalyst	H_2 Uptake (μmol/g)	Dispersion (%)	Metal area (m^2/g_{Cu})	Average Particle size (nm)
Cu/SBA-15	132	34	217	3.1
Cu/MCM-41	80	21	132	5.1
Cu/MCM-48	151	39	249	2.7
Cu/KIT-6	61	16	101	6.7

The SEM (Fig. 6) and TEM (Fig. 7) analysis were conducted to determine the morphologies (shape and size of the pore) of the mesoporous silica-supported copper catalysts. The SEM image of SBA-15 displayed a multiple rope like domains of relatively uniform in size structure. Further, the MCM-48 comprised of spherical particles with diameter ranging from 0.3 to 0.5 µm while pure KIT-6 support exhibited spherical platelets like morphology. The TEM images of Cu catalysts exhibited a well-defined ordered structure with different sizes and distribution. It was noticed that the mesoporous framework of the four samples retained their morphology even after impregnation with copper particles.

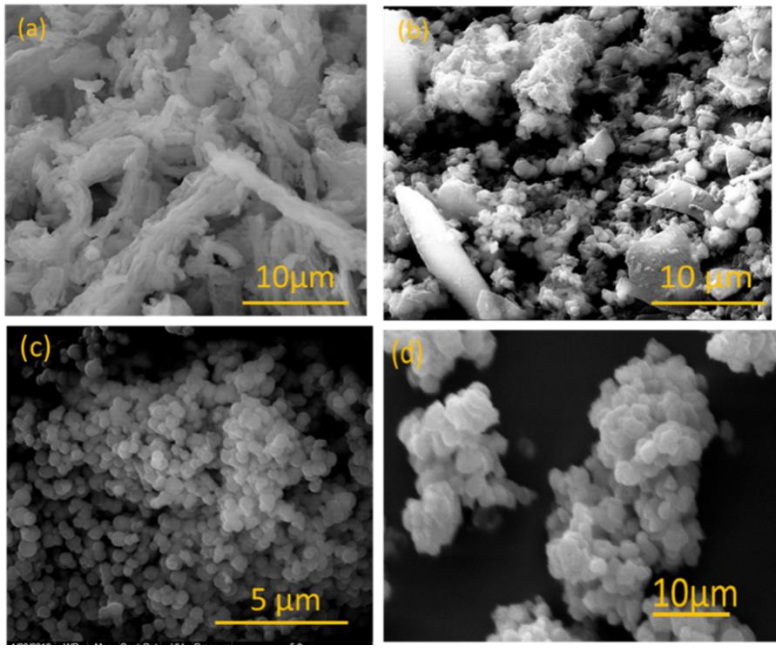

Figure 6.SEM images of (a) Cu/SBA-15 (b) Cu/MCM-41 (c) Cu/MCM-48 (d) Cu/KIT-6 catalysts.

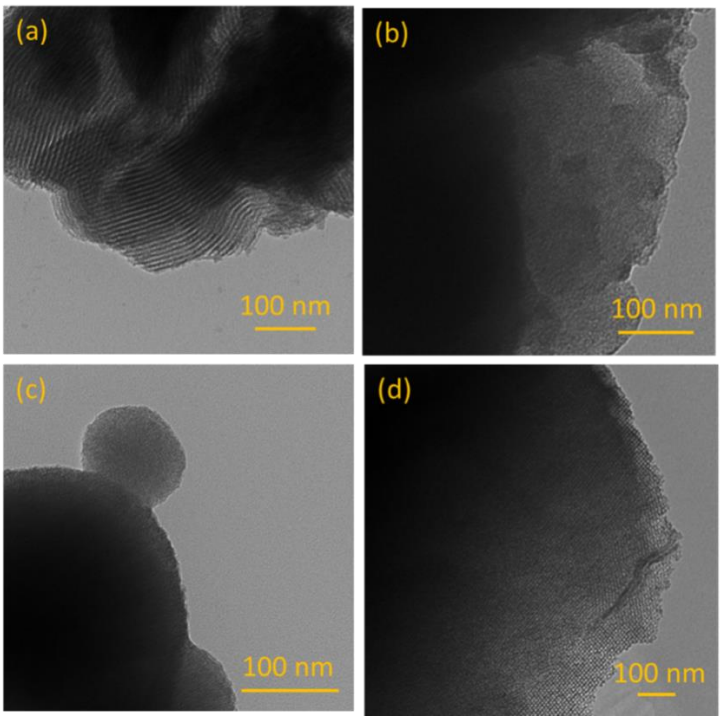

Figure 7. TEM images of (a) Cu/SBA-15 (b) Cu/MCM-41 (c) Cu/MCM-48 (d) Cu/KIT-6 catalysts.

The bare mesoporous silica supports morphologies and structural changes were also analysed by SEM and TEM analysis. The structure for all the supports were intact and there are no significant morphological changes after Cu incorporation (see supplementary information Figures S1 and S2).

Catalytic activity results

Evaluation of the catalytic activity of mesoporous silica-supported copper catalysts were conducted in a continuous fixed-bed reactor at 265°C and 0.1 MPa hydrogen pressure (Table 4). In LA hydrogenation, GVL was found to be the primary and desired product, whereas angelica lactone (AL) and valeric acid (VA) were produced as the by-products (Fig. 8). It was clearly evident that the, first LA was dehydrated to AL and then hydrogenated to GVL in the final stage. We selected 5 wt.% as the optimal Cu loading based on our previous studies. The catalytic hydrogenation of LA studied over bare supports under similar reaction conditions that of Cu supported catalysts. As we predicted that the bare mesoporous silica

support materials exhibit low activity due to absence of active sites. The LA conversion of maximum of below 12% were achieved over all the bare supports (Table A1). Angelic lactone is predominately as main product formed, and traces of amounts of GVL is noticed in the product stream.

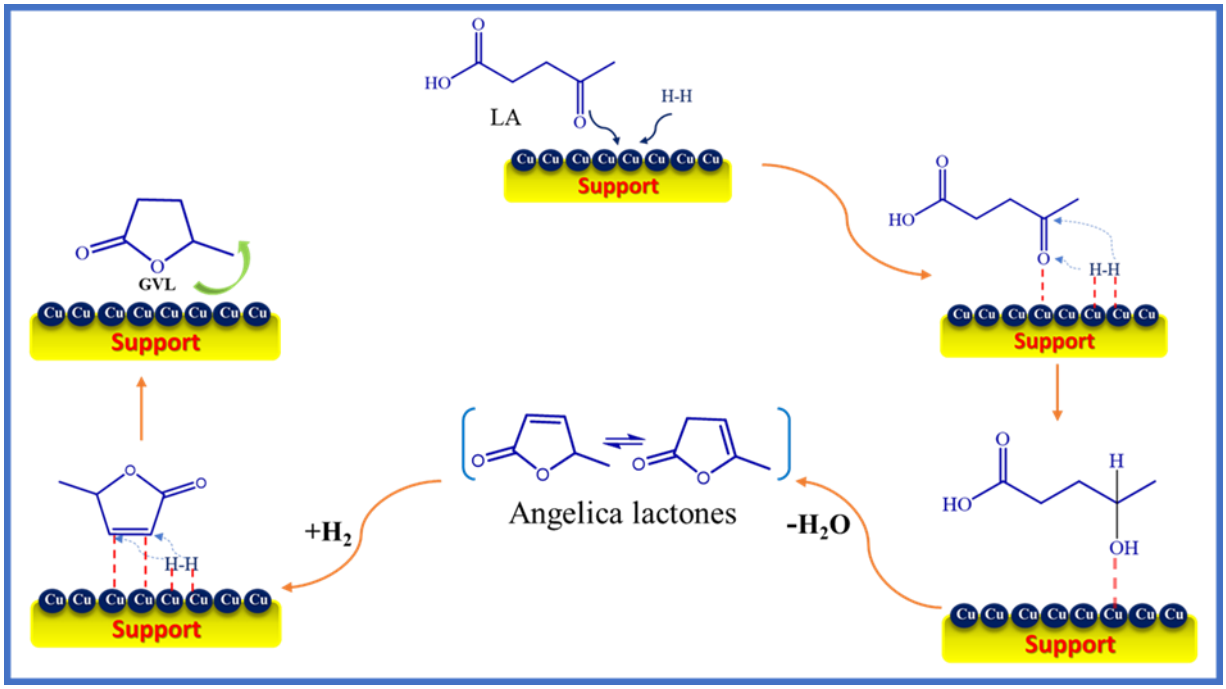

Figure 8. The reaction mechanism involved in the LA conversion to GVL over Cu-supported catalysts.

According to previous reports, over 5 wt.% Cu/SiO_2 shown complete conversion of LA with GVL selectivity of 94% and 6% of AL at 265°C and 0.1 MPa was obtained. Further, in another study, over 20 wt.% Cu/SiO_2 catalyst exhibited 73.4% LA conversion and 75.4% GVL selectivity at 250°C and WHSV of 3.30 h^{-1}[24]. In the present study, we achieved better results with low Cu loading compared to published data on Cu-based catalysts and overall, 5 wt.% Cu/SBA-15 exhibited complete conversion of LA with 98% GVL selectivity at 265°C temperature. Moreover, the Cu/MCM-48 catalyst has high active surface area, Cu dispersion and smaller Cu particle sizes compared to Cu/SBA-15, Cu/MCM-41, and Cu/KIT-6. In addition, Cu/MCM-48 showed higher metal surface area compared to

all, however, a lower catalytic activity was exhibited compared to Cu/SBA-15 catalyst. This indicated that, in case of Cu/MCM-48, a low surface acidity and also narrow pores could not render LA to the pore channels and led to low accessibility to the active sites compared to Cu/SBA-15. The conversion of LA over supported mesoporous silica catalyst was in the sequence of Cu/SBA-15>Cu/MCM-48>Cu/MCM-41>Cu/KIT-6. The order of the LA conversion was observed to be consistent with that of the total surface acidity, thus, highest LA conversion for Cu/SBA-15 catalyst was achieved. The superior catalytic activity was attributed to the availability of the highly reducible copper species over the surface and intrinsic of the mesoporous channels of the catalysts. Among all catalysts, 5 wt.% Cu/SBA-15 achieved superior performance and achieved complete LA conversion with ~98% GVL selectivity. Sakthivel et al. also reported among the different mesoporous supports, Sn/Al-SBA-15 showed highest LA conversion (~99%) and 100% selectivity towards the desired products (GVL) at 400°C in batch reactor [41] . The same group also reported 5% Ru/Zr/Al-SBA-15 catalyst exhibited the highest catalytic activity with ~97% LA conversion and ~84% selectivity towards methyl tetrahydrofuran (MTHF) at high temperature 400°C in batch reactor. Moreover, MTHF formed mostly *via* hydrogenation of GVL [42]**.**

Table 4. Catalytic performance of different mesoporous silica supported Cu catalysts including the reaction rate and turn over frequency (TOF).

Catalyst	Conversion (%)	Selectivity (%)				Rate (μmol. $g_{cat}^{-1}.s^{-1}$)	TOF (s^{-1})
		AL	GVL	VA	Others		
Cu/SBA-15	100	-	98	2	-	9.09	0.0385
Cu/MCM-41	85	16	77	3	4	7.73	0.0327
Cu/MCM-48	92	4	92	2	2	8.37	0.0354
Cu/KIT-6	78	29	69	1	1	7.09	0.0300

Reaction conditions: 10 wt.% of aqueous levulinic acid, 0.3 g catalyst, WHSV 0.550 h^{-1} and H_2 flow 30 mL min^{-1} under atmospheric pressure. VA = valeric acid and AL = angelica lactone.

Hydrogenation of LA over Cu/SBA-15, Cu/MCM-41, Cu/MCM-48 and Cu/KIT-6 was carried out at different reaction temperatures ranging from 225°C to 300°C (Fig. 8). Conversion of LA over the Cu/SBA-15, Cu/MCM-41, Cu/MCM-48 and Cu/KIT-6 catalysts increased from 77% to 100%, 58% to 98%, 64% to 100% and 48 to 88%, respectively, with the reaction temperatures from 225°C to 300°C. Moreover, complete LA conversion and 98% GVL selectivity was achieved at temperature around265°C over SBA/15 due to high reducibility and surface acidity. However, the selectivity for AL was typically very low at similar reaction temperature. Over Cu/SBA-15 and Cu/MCM-48 catalysts shown greater than 90% GVL selectivity with complete LA conversion, whereas Cu/KIT-6 exhibited low activity in terms of LA conversion and GVL selectivity. Moreover, the selectivity to GVL decreased and selectivity to VA increased with the temperature (from 265 to 300°C). This trend indicated that the higher temperatures (above 265°C) led to the dehydration reactions occur and thus, the formation rate from GVL to VA will be accelerated (at higher temperatures) . The high activity over Cu/SBA-15 is due to the correlation with acidity and Cu dispersion. As we can see from the Table 3. Cu/MCM-48 possessed high active surface area, Cu dispersion and smaller metallic Cu particle sizes compared to Cu/SBA-15, Cu/MCM-41, and Cu/KIT-6. In addition, Cu/MCM-48 showed higher metal surface area however, a lower catalytic activity was exhibited compared to Cu/SBA-15. This indicated that in case of Cu/MCM-48, a low surface acidity and narrow pores could not render LA to the pore channels and led to low accessibility to the active sites compared to Cu/SBA-15. This indicated that in case of Cu/MCM-48, a low surface acidity and narrow pores could not render LA to the pore channels and led to low accessibility to the active sites compared to Cu/SBA-15.

Previous studies concluded similar behavior for the Cu/Al_2O_3 catalyst, which accelerated the dehydration of LA molecules over the surface at high temperatures, resulting in the ring

opening of GVL molecules occur and thus, decreased the selectivity towards GVL. Apparently, initially, LA is converted to AL followed by its subsequent hydrogenation to GVL. Under the studied reaction conditions, in this work, the optimum reaction temperature for complete conversion of LA to GVL was 265°C. There are many copper-based catalytic systems reported in the literature with different Cu loadings over various support materials and reaction conditions. It is hard to compare all of them with our study due to variation in composition, and operating conditions. However, we collected few relevant data which had similar conditions to this work were summarised in Table 5 and short comparison between the reported Cu-based catalysts with this work was made. Recently, complete LA conversion can be achieved at mild temperature, *i.e.*, below 150°C but at high operating pressures **[43].** It was an evident that the trade-off factor between operating temperature and pressure are important thermodynamic constraints in the LA hydrogenation activity.

Table 5. Comparison of Cu based catalysts reported inthe literature (both batch and fixed bed reactors).

Catalyst	Reaction conditions	Hydrogen source & pressure	LA conversion (%)	GVL selectivity (%)	Reference
Cu/SiO_2 -Q6	T = 250°C, m = 0.75 g, LA:FA = 1:2	Formic acid	66	81	**[23]**
Cu-Ni/Al-Fe	T = 150°C, m = 0.125 g	H_2	95	70	**[21]**
8 wt.% Cu-12 wt.% Co/Al_2O_3	T = 250°C, m = 0.250 g	H_2	100	99	**[44]**
20% Cu/Al_2O_3	T = 240°C, m = 0.5 g	H_2	93.7	91.5	**[25]**
30% Cu–ZrO_2	T = 200°C, m = 0.05 g	H_2, 27 bar		90	**[45]**
3 wt.% $Cu/Zr_{0.8}$-$Ce_{0.2}$	T = 260°C, m = 0.5 g	Formic acid, 0.5 MPa	88.5	94.2	**[46]**
3 wt.% Cu/HTC*	T = 265°C, m = 0.5 g	H_2	87.5	95	**[47]**
4.7 wt.% Cu/ZrO_2-Al_2O_3	T = 130°C, m = 0.5 g	H_2, 3.0 MPa	100	100	**[48]**
3 wt.% B 18 wt.%Cu/ZrO_2	T = 150°C, m = 0.2 g	H_2, 3.0 MPa	100	100	**[41]**
32.3 wt% Cu/5%Al_2O_3-ZrO_2	T = 200°C, m = 0.05 g	H_2, 3.0 MPa	100	100	**[49]**

5 wt.% Cu/SBA-15	T = 265°C, m = 0.3 g	H_2, 0.1 MPa	100	98	This work

*HTC = hydrotalcite;

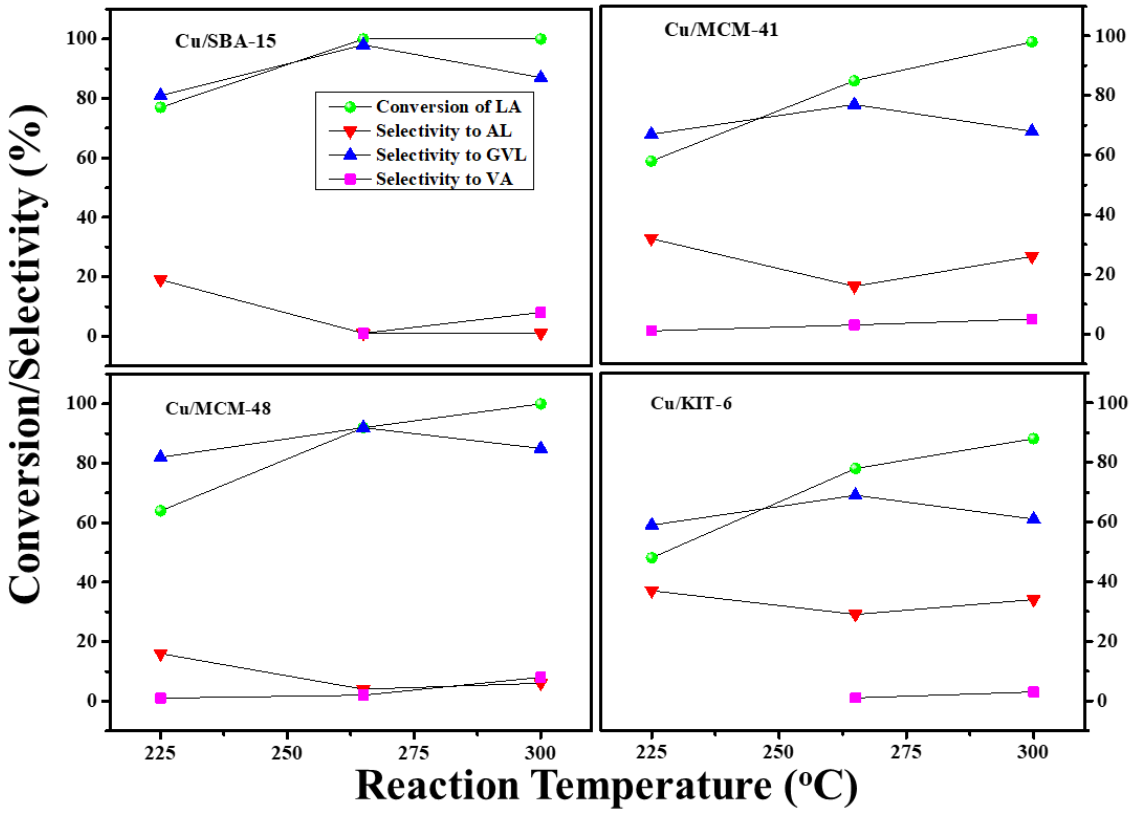

Figure 8. Effect of reaction temperature versus activity in LA conversion and selectivity over the various mesoporous silica supported copper catalysts.

Moreover, additional experiments were carried out to evaluate the stability of mesoporous silica-supported copper catalysts under time on stream (TOS) for 50 h (Fig. 9). Over Cu/SBA-15 catalyst, it was observed that it was more stable with complete LA conversion with negligible deactivation even after 30 h time on stream. For the Cu/MCM-41 catalyst, the LA conversion and selectivity was observed to be 85% and 77%, respectively, during 15 h reaction time. However, a drastic decrease in LA conversion (51%) and a slight decrease in GVL selectivity was observed as the TOS reached to 50 h. Over Cu/MCM-48 catalyst, the conversion of LA decreased linearly with TOS for the first 20 h approaching ~87% conversion, however, the activity decreased to 53% when further increasing TOS. The

reason behind the activity loss can be ascribed to the possible catalyst deactivation due to the blockage of the catalyst pores. Furthermore, for Cu/KIT-6, the LA conversion and GVL selectivity decreased rapidly during the initial 20 h under stream and attained only 40–50% conversion revealing continuous deactivation during the reaction time. Thus, stability studies of catalysts suggested that Cu/SBA-15 exhibited higher stability compared to Cu/MCM-41, Cu/MCM-48, and Cu/KIT-6 catalysts.

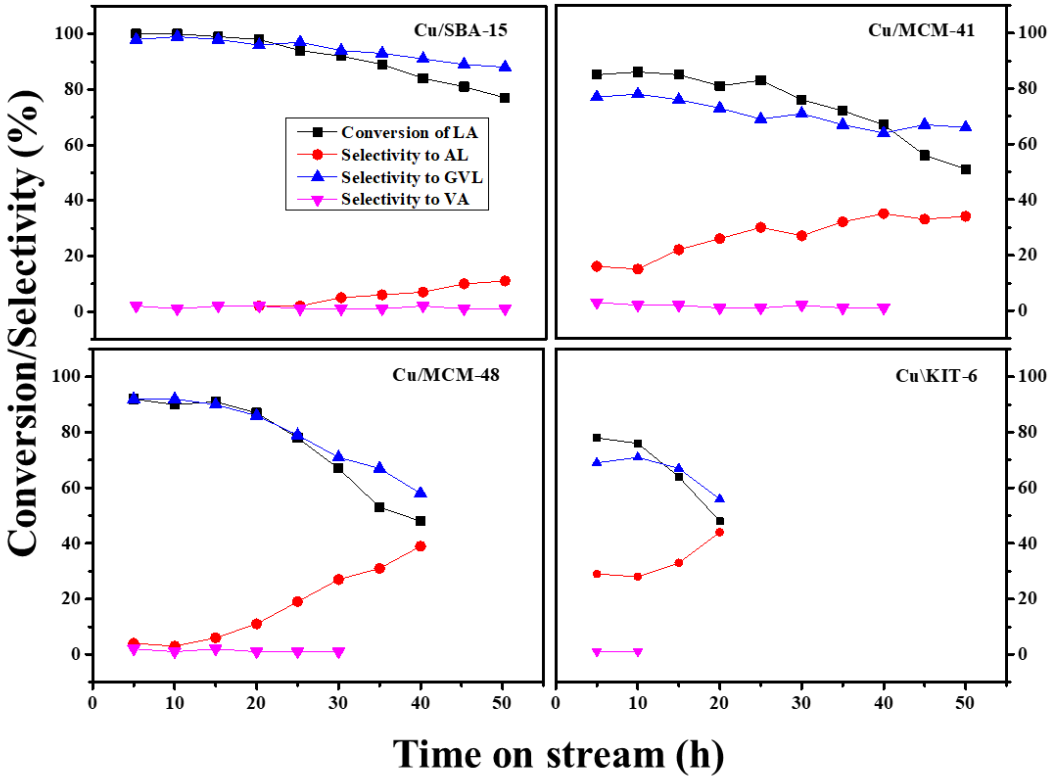

Figure 9. Time on stream studies of various mesoporous silica supported copper catalysts.

Conclusions

The vapor-phase hydrogenation of LA to GVL was carried out in a fixed-bed reactor over different mesoporous silica-supported copper catalysts at ambient hydrogen pressure. From the characterisation results, the diffraction patterns and N_2 adsorption-desorption studies revealed that the Cu impregnated catalysts retained their mesoporosity and the support structure was intact. Moreover, XRD results showed the presence of a highly dispersed CuO

species over all the catalysts except Cu/KIT-6. The support structure had a profound effect on the activity of the catalyst. The copper modified SBA-15 and MCM-48 had desired optimal properties and presented better performance compared to other catalysts. Overall, the Cu-SBA-15 catalyst exhibited the highest catalytic activity in terms of LA conversion (100%) and GVL selectivity (98%) compared to other prepared catalysts owing to its high surface acidity and Cu dispersion. The study further indicated that the copper surface area, acidity, and diffusion limitation of reactants into pore channels were the key factors, which influenced the activity of catalysts. The overall activity trend of different mesoporous silica-supported copper catalysts for the LA conversion was found to be in descending order: Cu-SBA-15>Cu-MCM-48>Cu-MCM-41>Cu-KIT-6.

Acknowledgments & funding

Dr. Putra Kumaracknowledgesthe Council of Scientific and Industrial Research (CSIR), New Delhi for the award of Senior Research Fellowship (SRF). Dr. Putra Kumar acknowledges funding provided by National Science Foundation of China (Project No.51871114) to carry out the research.

Conflicts of interest/Competing interests

There is no conflict of interest (not applicable).

References

1. Climent MJ, Corma A, Iborra S (2014) Conversion of biomass platform molecules into fuel additives and liquid hydrocarbon fuels. Green Chem 14:516–547. doi: 10.1039/c3gc41492b
2. Wenxiu Cao, Wenhao Luo, Hongguang Ge, Yang Su, Aiqin Wang and

TZ (2017) UiO-66 derived Ru/ZrO_2@C as a highly stable catalyst for hydrogenation of levulinic acid to γ-valerolactone. Green Chem 19:2201–2211. doi: 10.1039/C7GC00512A

3. Yang Y, Sun C, Brown DE, Zhang L, Yang F (2016) A smart strategy to fabricate Ru nanoparticle inserted porous carbon nano fi bers as highly e ffi cient levulinic acid hydrogenation catalysts †. Green Chem 18:3558–3566. doi: 10.1039/c5gc02802g
4. David MA, Jean MR, Max AM Stephanie GW, James AD (2013) Direct conversion of cellulose to levulinic acid and gamma-valerolactone using solid acid catalysts, Catal. Sci. Technol. 3: 927-931. doi: 10.1039/c2cy20689g
5. Touchy AS, Hakim Siddiki SMA, Kon K, Shimizu KI (2014) Heterogeneous Pt catalysts for reductive amination of levulinic acid to pyrrolidones. ACS Catal 4:3045–3050. doi: 10.1021/cs500757k
6. Yan K, Jarvis C, Gu J, Yan Y (2015) Production and catalytic transformation of levulinic acid: A platform for speciality chemicals and fuels. Renew Sustain Energy Rev 51:986–997. doi: 10.1016/j.rser.2015.07.021
7. Drew JB, Carlos AH, Jacob H, Christos CM, James AD (2011) Production of liquid hydrocarbon fuels by catalytic conversion of biomass-derived levulinic acid. Green Chem 13: 1755-1765. doi: 10.1039/c2cy20689g
8. Yan K, Yang Y, Chai J, Lu Y (2015) Catalytic reactions of gamma-

valerolactone: A platform to fuels and value-added chemicals. Appl Catal B Environ 179:292–304. doi: 10.1016/j.apcatb.2015.04.030

9. David MA, Stephanie GW, James AD (2013) Gamma-valerolactone, a sustainable platform molecule derived from lignocellulosic biomass. Green Chem 15: 584-595. doi:10.1039/c3gc37065h.

10. Dhanalaxmi K, Singuru R, Mondal S, Bai L, Reddy BM, Bhaumik A, Mondal J (2017) Magnetic Nanohybrid Decorated Porous Organic Polymer: Synergistic Catalyst for High Performance Levulinic Acid Hydrogenation. ACS Sustain Chem Eng 5:1033–1045. doi: 10.1021/acssuschemeng.6b02338

11. Gu XM, Zhang B, Liang HJ, Ge H Bin, Yang HM, Qin Y (2017) Pt/HZSM-5 catalyst synthesized by atomic layer deposition for aqueous-phase hydrogenation of levulinic acid to valeric acid. Ranliao Huaxue Xuebao/Journal Fuel Chem Technol 45:714–722. doi: 10.1016/s1872-5813(17)30035-x

12. Mustafin K, Cárdenas-Lizana F, Keane MA (2017) Continuous gas phase catalytic transformation of levulinic acid to γ-valerolactone over supported Au catalysts. J Chem Technol Biotechnol 92:2221–2228. doi: 10.1002/jctb.5258

13. Piskun AS, De Haan JE, Wilbers E, Van De Bovenkamp HH, Tang Z, Heeres HJ (2016) Hydrogenation of Levulinic Acid to γ-Valerolactone in Water Using Millimeter Sized Supported Ru Catalysts in a Packed Bed

Reactor. ACS Sustain Chem Eng 4:2939–2950. doi: 10.1021/acssuschemeng.5b00774

14. Yan K, Lafleur T, Jarvis C, Wu G (2014) Clean and selective production of γ-valerolactone from biomass-derived levulinic acid catalyzed by recyclable Pd nanoparticle catalyst. J Clean Prod 72:230–232. doi: 10.1016/j.jclepro.2014.02.056
15. Song S, Yao S, Cao J, Di L, Wu G, Guan N, Li L (2017) Heterostructured Ni/NiO composite as a robust catalyst for the hydrogenation of levulinic acid to γ-valerolactone. Appl Catal B Environ 217:115–124. doi: 10.1016/j.apcatb.2017.05.073
16. Sun P, Gao G, Zhao Z, Xia C, Li F (2014) Stabilization of cobalt catalysts by embedment for efficient production of valeric biofuel. ACS Catal 4:4136–4142. doi: 10.1021/cs501409s
17. Yuan J, Li SS, Yu L, Liu YM, Cao Y, He HY, Fan KN (2013) Copper-based catalysts for the efficient conversion of carbohydrate biomass into γ-valerolactone in the absence of externally added hydrogen. Energy Environ Sci 6:3308–3313. doi: 10.1039/c3ee40857d
18. Wettstein SG, Bond JQ, Alonso DM, Pham HN, Datye AK, Dumesic JA (2012) RuSn bimetallic catalysts for selective hydrogenation of levulinic acid to γ-valerolactone. Appl Catal B Environ 117–118:321–329. doi: 10.1016/j.apcatb.2012.01.033
19. Yan K, Chen A (2014) Selective hydrogenation of furfural and levulinic

acid to biofuels on the ecofriendly Cu-Fe catalyst. Fuel 115:101–108. doi: 10.1016/j.fuel.2013.06.042

20. Yang Y, Gao G, Zhang X, Li F (2014) Facile fabrication of composition-tuned Ru-Ni bimetallics in ordered mesoporous carbon for levulinic acid hydrogenation. ACS Catal 4:1419–1425. doi: 10.1021/cs401030u
21. Zhang R, Ma Y, You F, Peng T, He Z, Li K (2017) Exploring to direct the reaction pathway for hydrogenation of levulinic acid into Γ-valerolactone for future Clean-Energy Vehicles over a magnetic Cu-Ni catalyst. Int J Hydrogen Energy 42:25185–25194. doi: 10.1016/j.ijhydene.2017.08.121
22. Upare PP, Lee JM, Hwang YK, Hwang DW, Lee JH, Halligudi SB, Hwang JS, Chang JS (2011) Direct hydrocyclization of biomass-derived levulinic acid to 2-methyltetrahydrofuran over nanocomposite copper/silica catalysts. ChemSusChem 4:1749–1752. doi: 10.1002/cssc.201100380
23. Lomate S, Sultana A, Fujitani T (2017) Effect of SiO2 support properties on the performance of Cu-SiO2 catalysts for the hydrogenation of levulinic acid to gamma valerolactone using formic acid as a hydrogen source. Catal Sci Technol 7:3073–3083. doi: 10.1039/c7cy00902j
24. Yoshida R, Sun D, Yamada Y, Sato S, Hutchings GJ (2017) Vapor-phase hydrogenation of levulinic acid to Γ-valerolactone over Cu-Ni bimetallic catalysts. Catal Commun 97:79–82. doi: 10.1016/j.catcom.2017.04.018
25. Sun D, Ohkubo A, Asami K, Katori T, Yamada Y, Sato S (2017) Vapor-

phase hydrogenation of levulinic acid and methyl levulinate to Γ-valerolactone over non-noble metal-based catalysts. Mol Catal 437:105–113. doi: 10.1016/j.mcat.2017.05.009

26. Balla P, Perupogu V, Vanama PK, Komandur VRC (2016) Hydrogenation of biomass-derived levulinic acid to γ-valerolactone over copper catalysts supported on ZrO2. J Chem Technol Biotechnol 91:769–776. doi: 10.1002/jctb.4643

27. Putrakumar B, Nagaraju N, Kumar VP, Chary KVR (2015) Hydrogenation of levulinic acid to γ-valerolactone over copper catalysts supported on γ-Al2O3. Catal Today 250:209–217. doi: 10.1016/j.cattod.2014.07.014

28. Hoffmann F, Cornelius M, Morell J, Fröba M (2006) Silica-based mesoporous organic-inorganic hybrid materials. Angew Chemie - Int Ed 45:3216–3251. doi: 10.1002/anie.200503075

29. Patel A, Shukla P, Rufford T, Wang S, Chen J, Rudolph V, Zhu Z (2011) Catalytic reduction of NO by CO over copper-oxide supported mesoporous silica. Appl Catal A Gen 409–410:55–65. doi: 10.1016/j.apcata.2011.09.024

30. Fulvio PF, Pikus S, Jaroniec M (2010) SBA-15-supported mixed-metal oxides: Partial hydrolytic sol-gel synthesis, adsorption, and structural properties. ACS Appl Mater Interfaces 2:134–142. doi: 10.1021/am900625c

31. Abrokwah RY, Deshmane VG, Kuila D (2016) Comparative performance of M-MCM-41 (M: Cu, Co, Ni, Pd, Zn and Sn) catalysts for steam reforming of methanol. J Mol Catal A Chem 425:10–20. doi: 10.1016/j.molcata.2016.09.019

32. Zhao Q, Shen Y, Wang Q, Tian J, Zhou X, Jiang T (2013) A comparative investigation on the catalytic activity of H-Al-MCM-48 and H-Zr-MCM-48 mesoporous molecular sieve on alkylation of phenol with tert-butyl alcohol. Chem Eng J 230:124–132. doi: 10.1016/j.cej.2013.06.057

33. Prabhu A, Kumaresan L, Palanichamy M, Murugesan V (2009) Synthesis and characterization of aluminium incorporated mesoporous KIT-6: Efficient catalyst for acylation of phenol. Appl Catal A Gen 360:59–65. doi: 10.1016/j.apcata.2009.03.004

34. Frey AS, Hinrichsen O (2012) Comparison of differently synthesized Ni(Al)MCM-48 catalysts in the ethene to propene reaction. Microporous Mesoporous Mater 164:164–171. doi: 10.1016/j.micromeso.2012.07.015

35. Tüysüz H, Lehmann CW, Bongard H, Tesche B, Schmidt R, Schüth F (2008) Direct imaging of surface topology and pore system of ordered mesoporous silica (MCM-41, SBA-15, and KIT-6) and nanocast metal oxides by high resolution scanning electron microscopy. J Am Chem Soc 130:11510–11517. doi: 10.1021/ja803362s

36. Derrien G, Charnay C, Zajac J, Jones DJ, Rozière J (2008) Copper-containing monodisperse mesoporous silica nanospheres by a smart one-

step approach. Chem Commun 3118–3120. doi: 10.1039/b804593c

37. Chmielarz L, Kuśtrowski P, Dziembaj R, Cool P, Vansant EF (2006) Catalytic performance of various mesoporous silicas modified with copper or iron oxides introduced by different ways in the selective reduction of NO by ammonia. Appl Catal B Environ 62:369–380. doi: 10.1016/j.apcatb.2005.09.004

38. Chary KVR, Sagar GV, Naresh D, Seela KK, Sridhar B (2005) Characterization and reactivity of copper oxide catalysts supported on TiO2-ZrO2. J Phys Chem B 109:9437–9444. doi: 10.1021/jp0500135

39. Sagar GV, Rao PVR, Srikanth CS, Chary KVR (2006) Dispersion and reactivity of copper catalysts supported on Al 2O3-ZrO2. J Phys Chem B 110:13881–13888. doi: 10.1021/jp0575153

40. Subbaramaiah V, Srivastava VC, Mall ID (2013) Optimization of reaction parameters and kinetic modeling of catalytic wet peroxidation of picoline by Cu/SBA-15. Ind Eng Chem Res 52:9021–9029. doi: 10.1021/ie400124d

41 Sakthivel K, Sivakumar T, Mani D, Elangovan E, Thanigaivel V (2020) Catalytic transfer hydrogenation of levulinic acid to γ-valerolactone over Sn/Al-SBA-15 catalysts, New J. Chem 44: 8209-8222. doi: 10.1039/D0NJ01288B

42 Sakthivel K, Sivakumar T, Elangovan E, Mani D, Thanigaivel V, Mathivanan D (2020) Catalytic conversion of levulinic acid under noncorrosive conditions using Ru/Zr/Al-SBA-15 catalysts. Microporous and Mesoporous Materials 305: 110298. doi:10.1016/j.micromeso.2020.110298

43. Li JF, Zhao L, Li J, Li M, Liu CL, Yang RZ, Dong WS (2019) Highly selective synthesis of γ-valerolactone from levulinic acid at mild conditions catalyzed by boron oxide doped Cu/ZrO2 catalysts. Appl Catal A Gen 587:117244. doi: 10.1016/j.apcata.2019.117244

44. Yanase D, Yoshida R, Kanazawa S, Yamada Y, Sato S (2020) Efficient formation of γ-valerolactone in the vapor-phase hydrogenation of levulinic acid over Cu-Co/alumina catalyst. Catal Commun 139:105967. doi: 10.1016/j.catcom.2020.105967

45. Orlowski I, Douthwaite M, Iqbal S, Hayward JS, Davies TE, Bartley JK, Miedziak PJ, Hirayama J, Morgan DJ, Willock DJ, Hutchings GJ (2019) The hydrogenation of levulinic acid to Γ-valerolactone over Cu–ZrO2 catalysts prepared by a pH-gradient methodology. J Energy Chem 36:15–24. doi: 10.1016/j.jechem.2019.01.015

46. Mitta H, Perupogu V, Boddula R, Ginjupalli SR, Inamuddin, Asiri AM (2020) Enhanced production of γ-valerolactone from levulinic acid hydrogenation-cyclization over ZrxCe1-xO2 based Cu catalysts. Int J Hydrogen Energy 45:26445–26457. doi: 10.1016/j.ijhydene.2019.11.149

47. Mitta H, Seelam PK, Chary KVR, Mutyala S, Boddula R, Inamuddin, Asiri AM (2018) Efficient Vapor-Phase Selective Hydrogenolysis of Bio-Levulinic Acid to γ-Valerolactone Using Cu Supported on Hydrotalcite Catalysts. Glob Challenges 2:1800028. doi: 10.1002/gch2.201800028

48. Li J, Li M, Zhang C, Liu CL, Yang RZ, Dong WS (2020) Construction of mesoporous Cu/ZrO2-Al2O3 as a ternary catalyst for efficient synthesis of γ-valerolactone from levulinic acid at low temperature. J Catal 381:163–174. doi: 10.1016/j.jcat.2019.10.031

49. He D, He Q, Jiang P, Zhou G, Hu R, Fu W (2019) Novel Cu/Al2O3-ZrO2 composite for selective hydrogenation of levulinic acid to Γ-valerolactone. Catal Commun 125:82–86. doi: 10.1016/j.catcom.2019.03.029